Modeling of Cylindrical Dielectric Resonators in Rectangular Waveguides and Cavities

Xiao-Peng Liang, *Student Member, IEEE,* and Kawthar A. Zaki, *Fellow, IEEE*

***Abstract*—The mode matching method is used to accurately model a generalized cylindrical dielectric resonator structure in a rectangular waveguide or cavity. The field distributions of different modes in cavities are given. The resonant frequencies of the cavities are calculated and compared to the measured data, showing very good agreement. The resonator structure can be a dielectric disk resonator, a ring resonator, a dielectric resonator with support, etc. This structure can be used in filter design as the basic element, which provides very good mechanical stability. The slot coupling between cavities is also analyzed, showing some interesting results.**

I. Introduction

DIELECTRIC loaded resonators and filters are widely used in satellite communications. The dielectric resonators are usually axially loaded in cylindrical enclosures [1]. In this structure, it is difficult to support the resonators, especially for more than 4-pole dual or 2-pole single mode filters. For good mechanical stability, planar dielectric loaded resonators, i.e., the cylindrical DR which is held perpendicular to the axis of the filters in a rectangular enclosure, are proposed for dual mode filters [2]. However, modeling planar DR is a difficult problem which has not been treated in the literature. This paper presents a method for analyzing such structures.

The configuration of a planar DR loaded rectangular waveguide is shown in Fig. 1. To properly implement mode matching, the structures and discontinuities boundaries are required to be parallel to the axes of only one kind of coordinate system. When this is not the case, e.g., a cylindrical DR in a rectangular waveguide, classical mode matching becomes inapplicable. The point matching method [3]–[5] and moment method with point matching [6] are used, which is far less accurate than using the mode matching method. Image principles are used in [7] and [8], in which an infinite number of images of the cylinder with respect to the guide walls are taken to match the boundaries of the walls. The scattered fields of the cylinder are represented in terms of the waveguide modes to yield a general formula determining the scattering matrix of the system. This is an approximate, powerful method, but it is more complicated and less accurate than mode matching. The integral equation with Green's function is used in [9]. This method has already been successfully used in free-space scattering problems. However, adapted to waveguides, it becomes too complicated to solve practical problems. The equivalence principle is used in [10], which might be an alternative of mode matching, but with no advantage observed. In [11], the Bessel–Fourier series is used to obtain the mutual inner product integrations of a dielectric post loaded rectangular waveguide junction, in which the integration for each term of the series can be analytically calculated. In [11], the post extends from the bottom to the top of the waveguide, therefore, only TE_{m0} modes are considered.

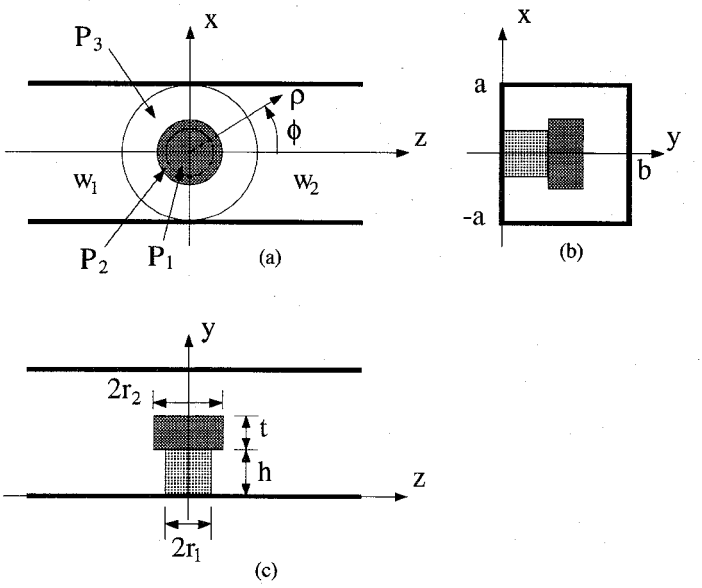

Fig. 1. Configuration of a generalized dielectric resonator with support in a rectangular waveguide.

In this paper, an approach similar to that in [11], with a generalized Bessel–Fourier series, is used to analyze the more general practical cylindrical structure shown in Fig. 1. Such a structure includes dielectric disk resonators, ring resonators, dielectric resonators with supports, etc.

Resonant frequencies and field distributions in DR loaded cavities are calculated. Measured data confirm the correctness and accuracy of the numerical results, showing very good agreement. As an application, the coupling of two identical planar DR loaded rectangular cavities through a rectangular slot, as shown in Fig. 2, is also calculated and compared to measured results.

Manuscript received March 26, 1993; revised June 15, 1993.

The authors are with the Electrical Engineering Department, University of Maryland, College Park, MD 20742.

IEEE Log Number 9213012.

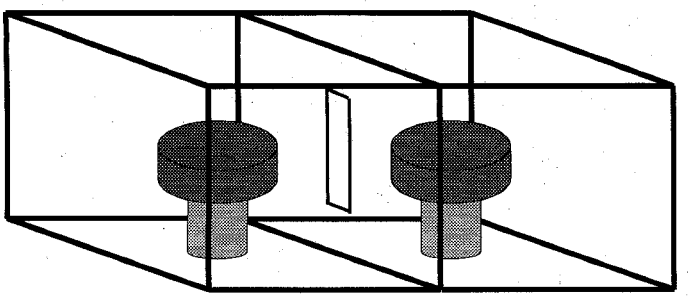

(a)

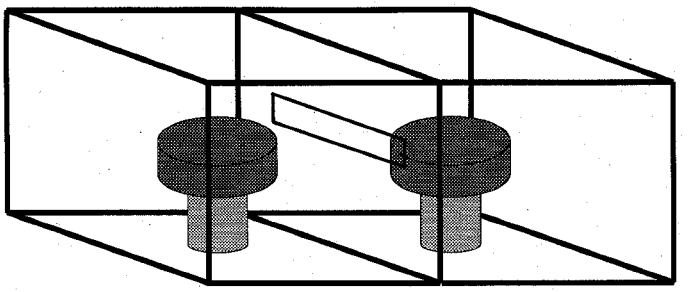

(b)

Fig. 2. Cylindrical dielectric resonator filter with (a) vertical slot coupling, and (b) horizontal slot coupling.

II. Scattering from a Cylindrical DR in a Rectangular Waveguide

The structure under consideration, shown in Fig. 1, consists of an infinite rectangular waveguide of cross section $2a \times b$, loaded with a dielectric cylindrical resonator of thickness t, diameter $2r_2$, supported by a concentric dielectric cylindrical tabular support of height h. The axis of the cylindrical dielectric structure coincides with the y-axis of a Cartesian coordinate system (x, y, z), and the rectangular waveguide walls are located at $x = \pm a$, and $y = 0, b$. The z-axis is normal to the cross section of the rectangular waveguide. A cylindrical coordinate system (ρ, ϕ, y) is defined by $\rho^2 = x^2 + z^2$, $\tan \phi = x/z$, as shown in Fig. 1. The structure of Fig. 1 is divided in two regions: region P, the cylindrical post region, defined as $\rho \leq a$; and region w, the rectangular waveguide region, defined as $\rho > a$; $-a < x < a$; $0 < y < b$. The cylindrical post region P is further subdivided into three subregions P_1, P_2 and P_3 defined as

$$P_1\colon\ \rho \leq r_1$$

$$P_2\colon\ r_1 \leq \rho \leq r_2$$

$$P_3\colon\ r_2 \leq \rho \leq a.$$

Finally, the waveguide region w is subdivided into subregions w_1 and w_2 defined as

$$w_1 \quad \rho > a;\ -a < x < a;\ 0 < y < b;\ z < 0$$

$$w_2 \quad \rho > a;\ -a < x < z;\ 0 < y < b;\ z > 0.$$

The fields in the post regions P_1, P_2, and P_3 are represented by a superposition of the modal functions in cylindrical coordinates (ρ, ϕ, y). These fields are expressed in terms of the multilayer parallel plate waveguides using the method described in [12]. Matching the boundary conditions at $\rho = r_1$ and r_2, which requires the tangential fields to be continuous, results in a matrix equation relating the modal field coefficients in region P_3 of the form

$$\begin{bmatrix} V_{11} & V_{12} & V_{13} & V_{14} \\ V_{21} & V_{22} & V_{23} & V_{24} \end{bmatrix} \begin{bmatrix} R^e \\ T^e \\ R^h \\ T^h \end{bmatrix} = 0 \tag{1}$$

where the V_s are submatrices whose elements are combinations of inner products of eigenfunctions of the fields in regions P_1, P_2, and P_3; R^e, T^e, R^h, and T^h are field coefficient vectors of eigenmodes in region P_3. The superscript e and h represent TM and TE eigenmodes (to the y-direction), respectively.

The tangential field components are matched on the imaginary boundary $\rho = a$ between region P_3 and the two waveguide regions w_1 and w_2. Due to the symmetry of the structure about the plane $x = 0$, perfect electric wall (PEW) or perfect magnetic wall (PMW) can be placed at this plane to simplify the problem. This process results in a matrix equation relating to the coefficient vectors of the incident and reflected normal mode fields in the two waveguide regions w_1 and w_2 to the field coefficient vectors of the eigenmodes in region P_3 of the form

$$\begin{bmatrix} W_{11} & W_{12} & \cdots & W_{18} \\ W_{21} & W_{22} & \cdots & W_{28} \\ W_{31} & W_{32} & \cdots & W_{38} \\ W_{41} & W_{42} & \cdots & W_{48} \end{bmatrix} \begin{bmatrix} A^{Ie} \\ A^{Ih} \\ A^{IIe} \\ A^{IIh} \\ B^{Ie} \\ B^{Ih} \\ B^{IIe} \\ B^{IIh} \end{bmatrix} = \begin{bmatrix} R^e \\ T^e \\ R^h \\ T^h \end{bmatrix} \tag{2}$$

where the W's are submatrices whose elements are expressed in terms of the inner products of modes at the imaginary boundary surface $\rho = a$. The A's and B's are the field coefficient vectors of the incident and reflected waves in the waveguide regions w_1 and w_2. When (2) is substituted into (1), a matrix equation relating the B's and A's can be obtained as

$$[B] = \begin{bmatrix} B^I \\ B^{II} \end{bmatrix} = [Q]^{-1}[P] \begin{bmatrix} A^I \\ A^{II} \end{bmatrix} = [S][A] \tag{3}$$

where matrix $[S]$ is the desired generalized scattering matrix of the waveguide discontinuity junction.

Because of the different coordinate systems at each side of the imaginary boundary, analytical integrations cannot be obtained directly for the mutual inner products. Instead of using numerical integrations that require a large amount

of CPU time, Bessel–Fourier series are used to derive two series, which can give analytical integration solutions in each term of the series. The two series are

$$\sin\left[\frac{m\pi}{2a}(\rho\sin(\phi)+a)\right]e^{\mp\gamma_{mi}\rho\cos(\phi)}=\sum_{n=-\infty}^{\infty}\sin\left(\frac{m\pi}{2}+n\phi\right)\cdot\begin{cases}J_n[T(\rho)]\exp[\mp jn\arctan(2a|\gamma_{mi}|/m/\pi)], & \gamma_{mi}^2<0\\ J_n[T(\rho)]\,[m\pi+2a\gamma_{mi})/(m\pi-2a\gamma_{mi})]^{\mp n/2}, & \gamma_{mi}^2>0,\ m\pi>2a|\gamma_{mi}|\\ (-1)^{n/2}I_n[|T(\rho)|]\,[(m\pi+2a\gamma_{mi})/(m\pi-2a\gamma_{mi})]^{\mp n/2}, & \gamma_{mi}^2>0,\ m\pi<2a|\gamma_{mi}|\end{cases}\tag{4a}$$

$$\cos\left[\frac{m\pi}{2a}(\rho\sin(\phi)+a)\right]e^{\mp\gamma_{mi}\rho\cos(\phi)}=\sum_{n=-\infty}^{\infty}\cos\left(\frac{m\pi}{2}+n\phi\right)\cdot\begin{cases}J_n[T(\rho)]\exp[\mp jn\arctan(2a|\gamma_{mi}|/m/\pi), & \gamma_{mi}^2<0\\ J_n[T(\rho)]\,[(m\pi+2a\gamma_{mi})/(m\pi-2a\gamma_{mi})]^{\mp n/2}, & \gamma_{mi}^2>0,\ m\pi>2a|\gamma_{mi}|\\ (-1)^{n/2}I_n[|T(\rho)|]\,[(m\pi+2a\gamma_{mi})/(m\pi-2a\gamma_{mi})]^{\mp n/2}, & \gamma_{mi}^2>0,\ m\pi<2a|\gamma_{mi}|\end{cases}\tag{4b}$$

$$T(\rho)=\frac{\rho}{2a}\sqrt{(m\pi)^2-4a^2\gamma_{mi}^2}\tag{4c}$$

$$\gamma_{mi}^2+k_0^2=\left(\frac{m\pi}{2a}\right)^2+\left(\frac{i\pi}{b}\right)^2.\tag{4d}$$

III. Cylindrical DR Loaded Rectangular Cavities

After the generalized scattering matrix of the cylindrical DR loaded rectangular waveguide junction is obtained, the cavity structure can be easily modeled by putting two perfect electric wall planes at $z=\pm L/2$ in Fig. 1 with $L>2r_2$. Shifting the reference planes of the obtained generalized scattering matrix to $z=\pm L/2$, the resonant frequencies of the cavity can be obtained as [13]

$$\det[\boldsymbol{S}+\boldsymbol{I}]=\boldsymbol{0}\tag{5}$$

where $[\boldsymbol{I}]$ is identity matrix. By increasing the maximum indices of modes in every dimension in each region of the structure, the numerical results should converge. Several test runs have shown that the maximum index in x and y directions in the waveguide regions of 6 and 10, respectively, is a proper choice. The maximum indices in ϕ and y directions in post regions are the same as in x and y directions in the waveguide regions, respectively. Once the resonant frequencies are calculated, the field coefficients in waveguide regions can be calculated through (5). All the other field coefficients in the other post regions can also be calculated. From these field coefficients in each region, the field distributions can be computed through the field expressions in the corresponding region.

Intuitively, the field patterns in the rectangular cavity should be close to those in the cylindrical cavity of equivalent parameters. Fig. 3 shows the electric field distributions of first *TE* mode in $x-z$ plane in the DR cross section. The *TE* mode is similar to that in cylindrical cavity structure. As expected, the electric fields form concentric loops as in the cylindrical cavity. Fig. 4 shows the magnetic field distributions of the first *TM* mode in the same $x-z$ plane as in Fig. 3. The magnetic fields form concentric loops as expected. Fig. 5(a) gives the electric field distributions of the first *HE* mode in $x-z$ plane at $y=0.4''$ with PEW and PMW at $x=0$ plane. Fig. 5(b) gives the magnetic field distributions of the same mode in the same plane. As it is shown, the *HE* modes with PEW and PMW at $x=0$ are degenerate modes. Fig. 5(c) gives the magnetic field distributions of *HE* mode in $x-y$ plane at $z=-0.5''$, which is at the end conductor plane.

For the resonant frequencies, again intuitively, the cylindrical DR in square cavities should give close results to those in cylindrical cavities, if the dielectric constant of the DR is high. Figs. 6 and 7 compare the results of the resonant frequencies of the two kinds of cavities with the variation of DR dielectric constant for three different modes. The cylindrical cavity diameter is taken to be the same as the square cavity width ($2a$) and length (L). As expected, the results from the two kinds of cavities are very close. Fig. 8 shows the effects of the support dielectric constant on the resonant frequencies. Fig. 9 shows the effects of the cavity length on the resonant frequencies. When increasing the cavity length, the resonant frequency with PEW at $x=0$ plane decreased as expected, however, the one with PMW increased.

Table I gives the comparison of the calculated and measured resonant frequencies on three different DR's. Good agreement is achieved.

IV. Slot Coupling for Filter Applications

The main application of the cavity structure discussed in this paper is its use as a basic filter element. Estimating the coupling between two adjacent cavities is the key to successfully designing a filter. The coupling structures, as shown in Fig. 2, consist of two identical cavities with a vertical/horizontal rectangular slot inserted in between.

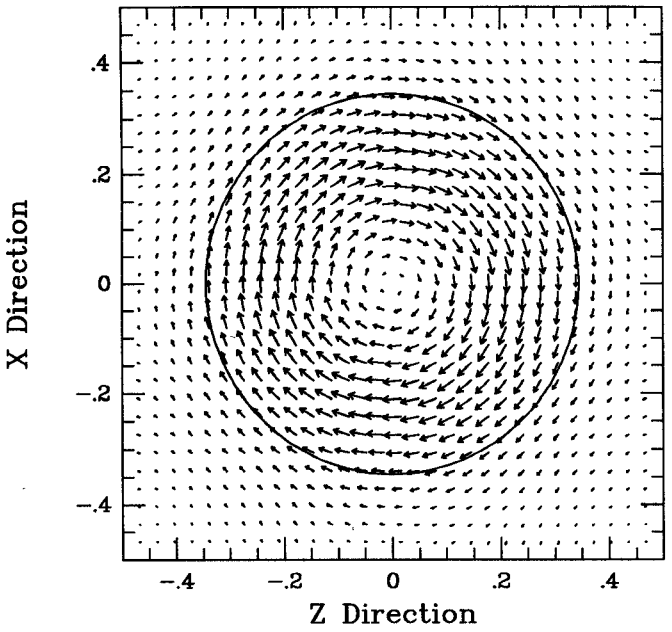

Fig. 3. Electric field distributions for the first *TE* mode at $y = 0.4''$ with $2a = 1''$, $b = 1''$, $2r_1 = 0''$, $2r_2 = 0.689''$, $h = 0.275''$, $t = 0.23''$, $L = 1''$, and $\epsilon_r = 38$.

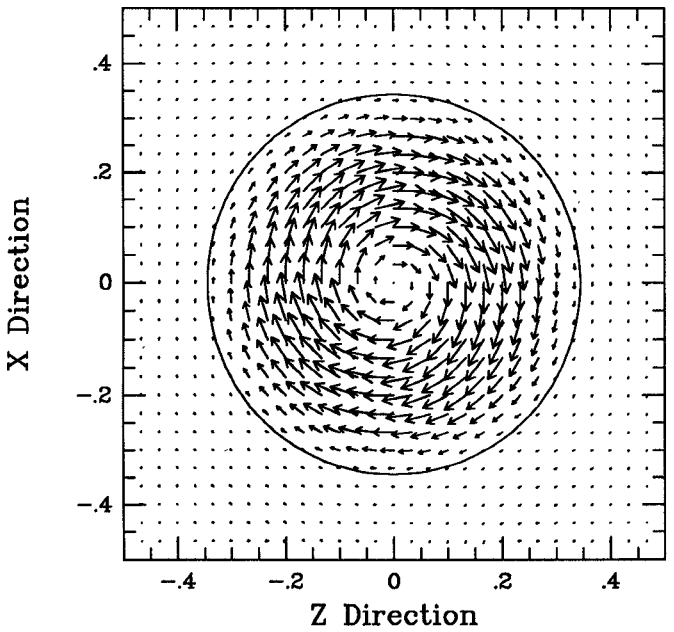

Fig. 4. Magnetic field distributions for the first *TM* mode at $y = 0.4''$ with $2a = 1''$, $b = 1''$, $2r_1 = 0''$, $2r_2 = 0.689''$, $h = 0.275''$, $t = 0.23''$, $L = 1''$, and $\epsilon_r = 38$.

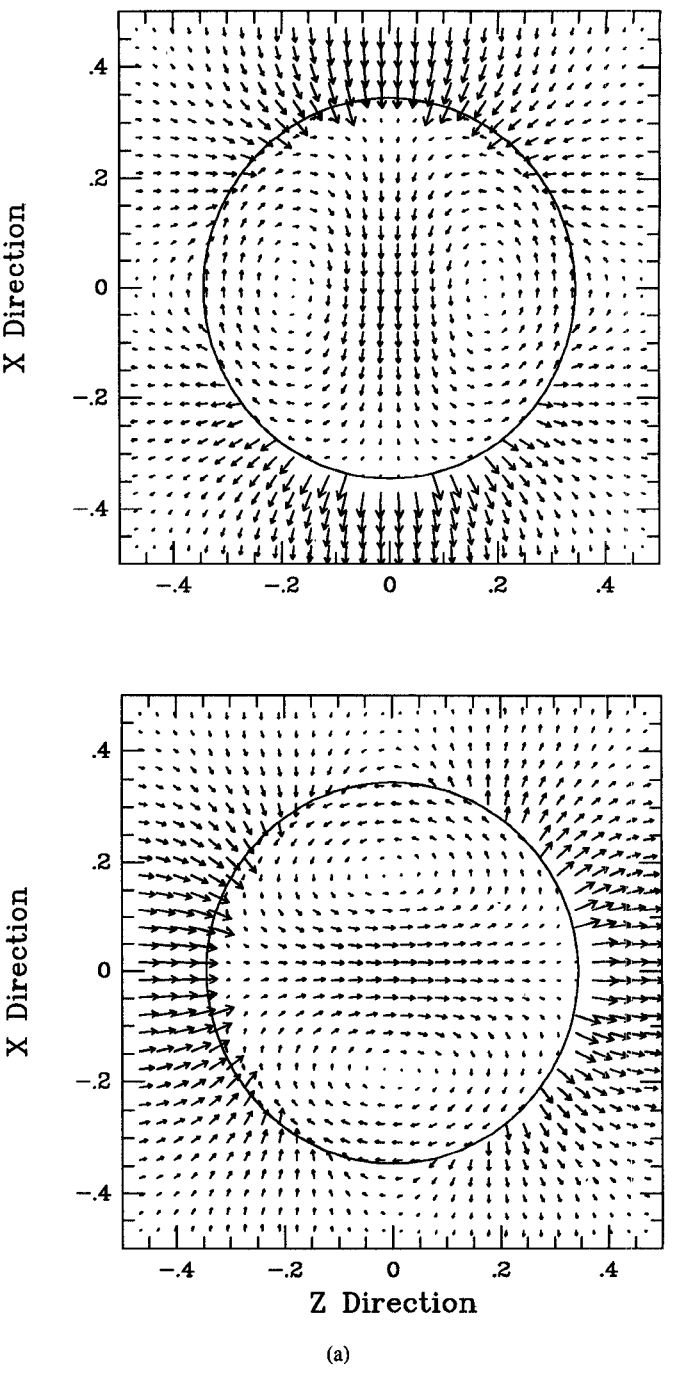

Fig. 5. (a) Electric field distributions for the first *HE* mode at $y = 0.4''$ with $2a = 1''$, $b = 1''$, $2r_1 = 0''$, $2r_2 = 0.689''$, $h = 0.275''$, $t = 0.23''$, $L = 1''$, $\epsilon_r = 38$; PEW for the upper one, and PMW for the lower one. (b) Magnetic field distributions for the first *HE* mode at $y = 0.4''$ with $2a = 1''$, $b = 1''$, $2r_1 = 0''$, $2r_2 = 0.689''$, $h = 0.275''$, $t = 0.23''$, $L = 1''$, $\epsilon_r = 38$; PEW for the upper one, and PMW for the lower one. (c) Magnetic field distributions for the first *HE* mode at $z = -0.5''$ with $2a = 1''$, $b = 1''$, $2r_1 = 0''$, $2r_2 = 0.689''$, $h = 0.275''$, $t = 0.23''$, $L = 1''$, $\epsilon_r = 38$; PEW for the upper one, and PMW for the lower one.

The rectangular slot between the two cavities creates two waveguide discontinuities connected back to back by a length of evanescent mode waveguide. These two waveguide discontinuities can be modeled by mode matching as in [14]. Cascading the generalized scattering matrices of the cylindrical DR loaded rectangular junctions and the waveguide discontinuities [13], as shown in Fig. 10, the resonant frequencies f_e and f_m of the coupled structure can be calculated from (5). Here, f_e and f_m are calculated by putting PEW and PMW, respectively, at the symmetric plane $A - A$. Then the coupling coefficient can be simply calculated as

$$k = \frac{M}{L} = \frac{f_e^2 - f_m^2}{f_e^2 + f_m^2}. \tag{6}$$

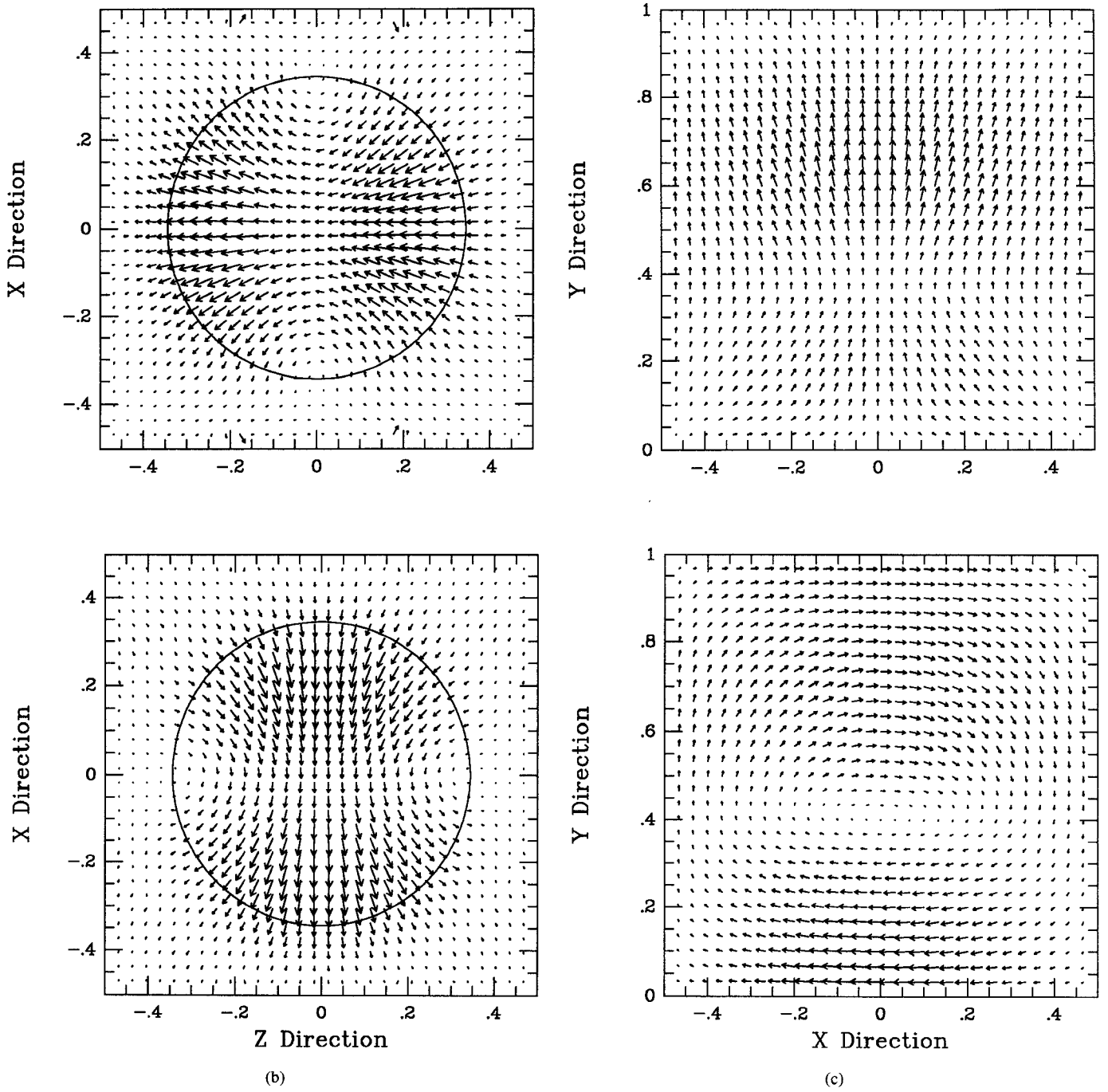

(b) (c)

Fig. 5. (*Continued.*)

Tangential magnetic fields in $x - y$ plane at the slot position are the main fields that produce the coupling. From Fig. 5(c), the tangential magnetic fields of the *HE* mode with PEW at $x = 0$ plane are mainly in the y direction, therefore, strong coupling is expected for vertical slot and almost zero coupling for horizontal slot. On the other hand, the fields of the *HE* mode with PMW at $x = 0$ plane are forming loops, strong coupling is expected for horizontal slot, and almost zero coupling for vertical slot. Fig. 11 shows the variation of the coupling coefficients with the vertical slot length. The measured data are also given, showing good agreement. Fig. 12 shows the variation of the coupling coefficients with the horizontal slot length. Although the same trend between calculated and measured data is obtained, there is an unexplained discrepancy between them, which is currently under investigation.

V. Conclusions

Accurate modeling of cylindrical dielectric resonators in rectangular waveguides and cavities is presented. The mode matching method is used with the derived Bessel–

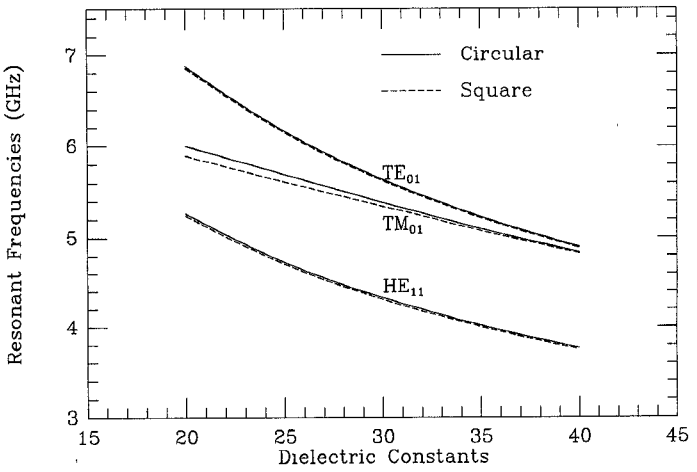

Fig. 6. Resonant frequencies of a dielectric disk on the bottom of a square cavity with $2a = 1''$, $b = 0.5''$, $2r_1 = 0''$, $2r_2 = 0.5''$, $h = 0''$, $t = 0.2''$, and $L = 1''$.

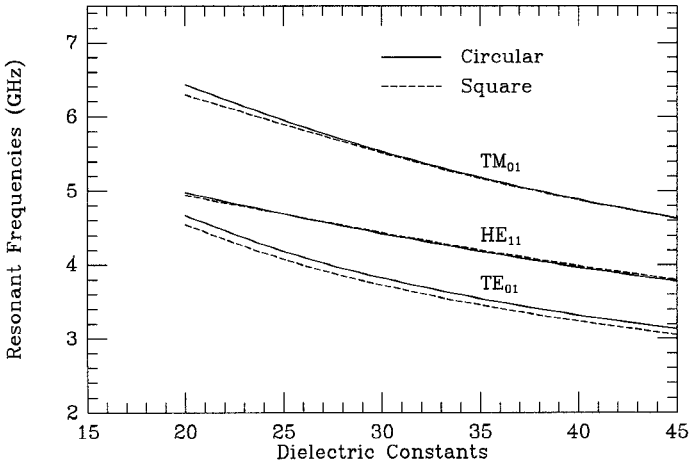

Fig. 7. Resonant frequencies of a dielectric disk placed off the bottom of a square cavity with $2a = 1''$, $b = 1''$, $2r_1 = 0''$, $2r_2 = 0.7''$, $h = 0.275''$, $t = 0.24''$, and $L = 1''$.

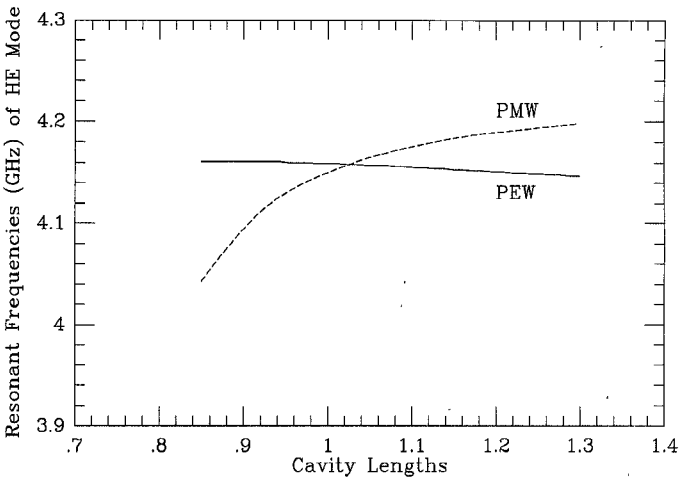

Fig. 9. Cavity length effect on the resonant frequencies with $2a = 1''$, $b = 1''$, $2r_1 = 0''$, $2r_2 = 0.689''$, $h = 0.275''$, $t = 0.23''$, $L = 0.92''$, and $\epsilon_r = 38$.

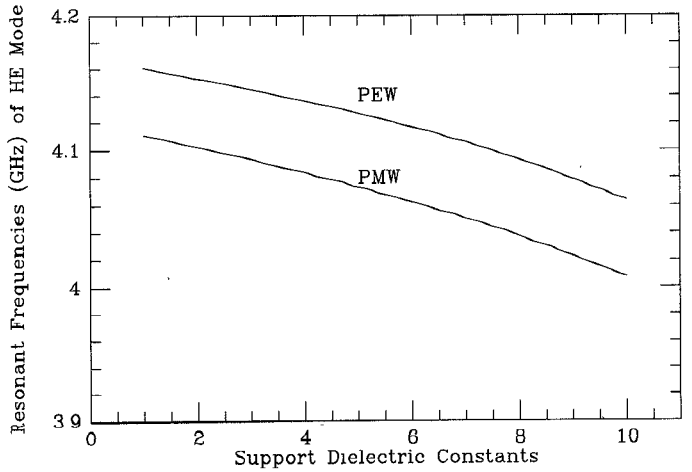

Fig. 8. Resonant frequencies of a dielectric disk with support with $2a = 1''$, $b = 1''$, $2r_1 = 0''$, $2r_2 = 0.689''$, $h = 0.276''$, $t = 0.23''$, $L = 0.92''$, and $\epsilon_r = 38$.

TABLE I
COMPARISON OF CALCULATED AND MEASURED RESONANT FREQUENCIES
$2a = 1''$, $b = 1''$, $2r_1 = 0$, $h = 0.275''$, $L = 0.92''$, and $\epsilon_r = 38$

$2r_2$ (inch)	t (inch)	Calculated	Measured
0.654	0.218	4.3880	4.382
0.689	0.230	4.1605	4.153
0.757	0.253	3.721	3.777

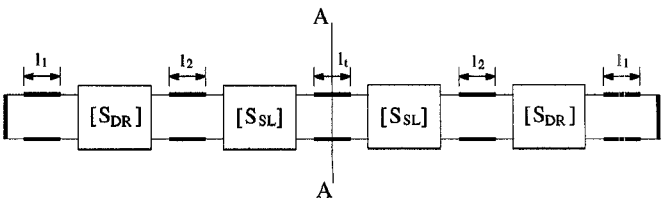

Fig. 10. Equivalent scattering matrix network of two cavities coupled through a rectangular slot. l_t—slot thickness, l_1—distance from DR to end, l_2—distance from DR to slot.

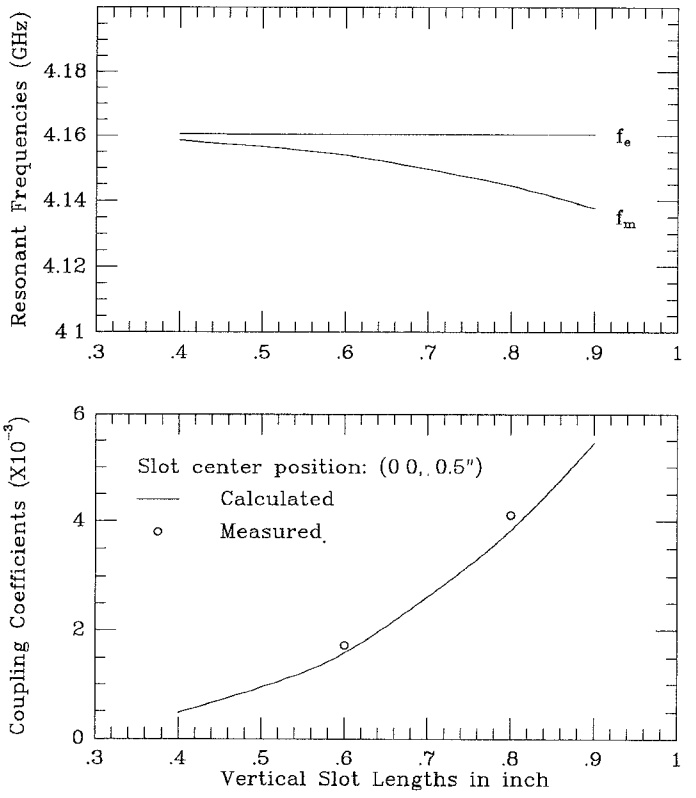

Fig. 11. Coupling coefficients versus vertical slot lengths with $2a = 1''$, $b = 1''$, $2r_1 = 0''$, $2r_2 = 0.689''$, $h = 0.276''$, $t = 0.23''$, $L = 0.92''$, $\epsilon_r = 38$, $l_w = 0.1''$, and $l_t = 0.032''$. l_w—slot width, l_t—slot thickness.

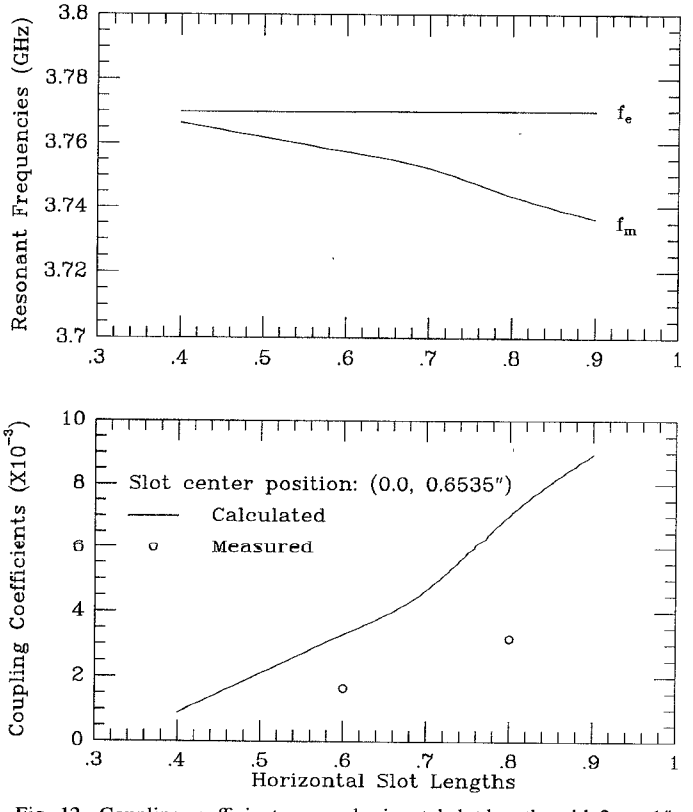

Fig. 12. Coupling coefficients versus horizontal slot lengths with $2a = 1''$, $b = 1''$, $2r_1 = 0''$, $2r_2 = 0.757''$, $h = 0.275''$, $t = 0.253''$, $L = 1.0125''$, $\epsilon_r = 38$, $l_w = 0.1''$, and $l_t = 0.032''$. l_w—slot width, l_t—slot thickness.

Fourier series for analytical integrations of the mutual inner products at the imaginary boundary. The generalized scattering matrix of the cylindrical DR loaded rectangular waveguide junction is given. Cavity resonators are analyzed by using the scattering matrix of the loaded waveguide, and the resonant frequencies and field distributions for different modes are computed. The calculated and measured data are compared, showing good agreement. The slot couplings between two identical cylindrical DR loaded rectangular cavities are also analyzed. The coupling results are important for filter application. Comparison of the calculated and measured data shows good agreement for vertical slot couplings and the same trend for horizontal slot couplings. Because of its good mechanical stability, this kind of DR loaded resonator and filter has strong potential application in satellite communications.

References

[1] S. J. Fiedziusko, "Dual-mode dielectric resonator loaded cavity filters," *IEEE Trans. Microwave Theory Tech.*, vol. MTT-30, pp. 1311–1316, Sept. 1982.

[2] C. M. Kudsia, R. Cameron, and W.-C. Tang, "Innovations in microwave filters and multiplexing networks for communications satellite systems," *IEEE Trans. Microwave Theory Tech.*, vol. MTT-40, pp. 1133–1149, June 1992.

[3] E. D. Nielsen, "Scattering by a cylindrical post of complex permittivity in a waveguide," *IEEE Trans. Microwave Theory Tech.*, vol. MTT-17, pp. 148–153, Mar. 1969.

[4] M. E. El-Shandwily, A. A. Kamal, and E. A. F. Abdallah, "General field theory treatment of E-plane waveguide junction circulators—Part I: Full-height ferrite configuration," *IEEE Trans. Microwave Theory Tech.*, vol. MTT-25, pp. 784–793, Sept. 1977.
[5] —, "General field theory treatment of E-plane waveguide junction circulators—Part II: Two-disk ferrite configuration," *IEEE Trans. Microwave Theory Tech.*, vol. MTT-25, pp. 794–803, Sept. 1977.
[6] Y. Leviatan and G. S. Sheaffer, "Analysis of inductive dielectric posts in rectangular waveguide," *IEEE Trans. Microwave Theory Tech.*, vol. MTT-35, pp. 48–58, Jan. 1987.
[7] N. Okamoto, I. Nishioka, and Y. Nakanishi, "Scattering by a ferromagnetic circular cylindrical in a rectangular waveguide," *IEEE Trans. Microwave Theory Tech.*, vol. MTT-19, pp. 521–527, June 1971.
[8] G. Cicconi and C. Rosatelli, "Solutions of the vector wave equation for inhomogeneous dielectric cylinders—Scattering in waveguide," *IEEE Trans. Microwave Theory Tech.*, vol. MTT-25, pp. 885–892, Nov. 1977.
[9] A. S. Omar and K. Schünemann, "Scattering by material and conducting bodies inside waveguides, Part I: Theoretical formulations," *IEEE Trans. Microwave Theory Tech.*, vol. MTT-34, pp. 266–271, Feb. 1986.
[10] Y. Y. Tsai and A. S. Omar, "Analysis of E-plane waveguide junction with partial height dielectric and ferrite inserts," in *1992 IEEE MTT-S Dig.*, pp. 309–312.
[11] R. Gesche and N. Löchel, "Scattering by a lossy dielectric cylinder in a rectangular waveguide," *IEEE Trans. Microwave Theory Tech.*, vol. MTT-36, pp. 137–144, Jan. 1988.
[12] S.-W. Chen and K. A. Zaki, "Dielectric ring resonators loaded in waveguide and on substrate," *IEEE Trans. Microwave Theory Tech.*, vol. MTT-39, pp. 2069–2076, Dec. 1991.
[13] X.-P. Liang, K. A. Zaki, and A. E. Atia, "Dual mode coupling by square corner cut in resonators and filters," *IEEE Trans. Microwave Theory Tech.*, vol. MTT-40, pp. 2294–2302, Dec. 1992.
[14] H.-C. Chang and K. A. Zaki, "Evanescent-mode coupling of dual mode rectangular waveguide filters," *IEEE Trans. Microwave Theory Tech.*, vol. MTT-39, pp. 1307–1312, Aug. 1991.

Xiao-Peng Liang, for a photograph and biography, see this issue, p. 2173.

Kawthar A. Zaki, (SM'85–F'91) for a photograph and biography, see this issue, p. 2173.